PHYSICAL REVIEW B VOLUME 47, NUMBER 20 15 MAY 1993-II

Surface reconstructions in the Ag/Si(111) system

K. J. Wan, X. F. Lin, and J. Nogami*

Department of Physics and the Laboratory for Surface Studies, University of Wisconsin–Milwaukee, Milwaukee, Wisconsin 53201

(Received 29 June 1992)

The behavior of silver on the Si(111) surface has been studied as a function of overlayer coverage and deposition conditions using scanning tunneling microscopy (STM) and low-energy electron diffraction. We examine how the different roles of Ag coverage and thermal annealing history determine surface ordering phenomena and atomic structure in this system. A growth phase diagram based on STM observations is presented. This diagram contains the well-known $\sqrt{3}\times\sqrt{3}$ and 3×1 reconstructions, as well as a phase characterized by 5×2 periodicity. Possible surface atomic arrangements for each phase are discussed based on the STM observations.

I. INTRODUCTION

The growth of silver on the (111) surface of silicon has been the focus of many studies over the past twenty years. This system has been regarded as a prototypical metal-semiconductor interface. This is due partially to the fact that there is limited reaction or intermixing between the two species. Although this simplifies some aspects of the interaction between the overlayer and substrate at the surface or interface, there are several aspects of the Ag/Si(111) system that have remained unresolved.

LeLay has written a comprehensive review which summarizes most of the work before 1983.[1] Ag growth proceeds in a layer-by-layer-like fashion at room temperature (RT) with the overlayer showing features characteristic of bulk Ag after a few monolayers. Above about 200 °C, the growth process turns to a Stranski-Krastanov mode: at approximately one monolayer (ML), the surface structure is characterized by a $\sqrt{3}\times\sqrt{3}$ periodicity and further deposition results in the nucleation of three-dimensional (3D) Ag crystallites. In the submonolayer region, the $\sqrt{3}\times\sqrt{3}$ phase undergoes a transformation to a 3×1 structure when the surface is annealed at temperatures high enough to induce some desorption of Ag.[1] This 3×1 structure converts to a 6×1 structure upon cooling to RT. The atomic arrangements for either of these structures has not been totally solved. The $\sqrt{3}\times\sqrt{3}$ phase, in particular, has been under intense study for many years with a wide variety of surface analytical techniques, including scanning tunneling microscopy (STM).[2–11] Comparatively little is known about the 3×1 structure.

In this study we present extensive STM results for Ag coverages up to 1 ML and thermal annealing above 300 °C. Large area STM images are used to address general growth phenomena on the 50 to 500 Å length scale. Some correspondence with previous work is established, particularly with regard to the phase diagram of surface behavior versus both Ag coverage and annealing temperature. Higher magnification images are used to study the atomic structure of the three ordered surface reconstructions observed here: $\sqrt{3}\times\sqrt{3}$, 3×1 (6×1), and a previously unknown 5×2 phase. Some of our results on the $\sqrt{3}\times\sqrt{3}$ phase have appeared elsewhere; these results support a particular atomic model.[12] Detailed images of the 3×1 and 5×2 phases are shown. A model for the 3×1 phase is proposed on the basis of some of these images.

II. EXPERIMENTAL METHODS

The STM and vacuum system used are commercially available.[13] The ultrahigh-vacuum chamber has a base pressure of 8×10^{-11} Torr, and is equipped with a four-grid low-energy electron diffraction (LEED) optics, which was used to monitor the surface structure. The chamber is also equipped with facilities for sample cleaning and annealing and metal deposition. In this system, samples and tips can be transferred to the chamber through load lock and introduced to the STM stage.

The Si(111) wafers were *n* type (phosphorous doped), oriented to within 15 in. of the (111) direction. The $12\times4\times0.4$ mm^3 samples were mounted on Ta supports, and held by a pair of Ta clips which were separated from the sample by additional Si spacers cut from the same wafer. Samples were cleaned by flashing them to 1150 °C for approximately 2 min and holding them at 1000 °C for about 10 min before gradually cooling down to RT. Both STM and LEED show the characteristic 7×7 periodicity of the clean surface.

The Ag films were deposited onto the substrate by sublimation from high-purity polycrystalline Ag material held in a shielded tungsten wire basket. A slow deposition rate (typically 0.05 ML/min) was used, where 1 ML corresponds to 7.83×10^{14} atoms/cm^2, the atomic density of a bulk-terminated Si(111) 1×1 surface. The thickness of the films was monitored with a quartz-crystal oscillator (QCO), which could be moved directly in front of the Ag source. The coverage of Ag was determined by timed exposure to the source. We also calibrated the coverage by simply counting the density of Ag-related features on the surface seen in the STM images at RT, where the Ag atoms are expected to stay on the surface. By doing this for many images, the coverage calibration statistically reached a certain degree of accuracy and was shown to be consistent with the QCO monitor.

The surfaces were annealed by either dc current heating, or by a separate filament heater which was located close to the sample holder. The filament provided more reproducible annealing at lower temperatures. The temperature was measured by both a thermocouple and by an optical pyrometer for temperatures higher than 550 °C. Below 550 °C, the temperature was determined from the power applied to the heater and the annealing time, which were previously calibrated against the sample temperature. The calibration was made by a separate measurement in which a thermocouple was directly mounted to the sample surface.

All STM measurements were carried out at RT. Thermal drifts during data acquisition cause the distortion of the images from their expected threefold symmetry. The images shown here have been corrected for this distortion by skewing the image appropriately. No other image processing of the data has been done except where explicitly noted when it was necessary to adjust the contrast in the image.

III. RESULTS AND DISCUSSION

A. Room-temperature behavior

We have studied the evolution of the surface morphology for RT Ag deposition for coverages up to 1 ML. LEED shows a gradual disappearance of the 7×7 pattern as the coverage approaches 1 ML, with no new superstructures evident without annealing the sample. Figure 1 shows an empty-state image at a nominal coverage of 0.5 ML.

This image shows the same behavior as in an earlier study by Tosch and Neddermeyer.[14] In the initial stages of adsorption, the Ag forms small triangular islands preferentially on the faulted half of the 7×7 unit cell. These islands vary somewhat in size but at these low coverages, they are all individually bounded by the borders of the 7×7 unit cell. Two shapes of these islands are most common. A smaller type, labeled "*A*," appears to leave the corner adatoms at least partially exposed. A second, slightly larger type labeled "*B*" covers the entire half of a unit cell. This might indicate preferential adsorption sites for Ag within each 7×7 unit cell, with some preference for adsorption at the rest atom sites. A type "*A*" island might involve only the rest atoms and perhaps the adjacent center adatoms, whereas a type "*B*" island appears to involve all the adatom sites. Preferential metal adsorption on rest atom sites has been observed previously for both Sn and Pb on Si(111).[15,16] Preferential reaction of the faulted half has also been seen after Pd deposition.[17]

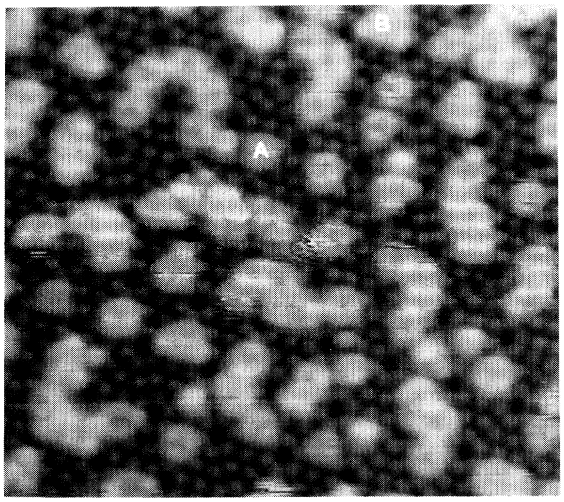

FIG. 1. Empty-state image of 0.5 ML Ag on Si(111) 7×7, deposited at room temperature. Two types of islands are labeled "*A*" and "*B*."

As the coverage increases, the Ag gradually forms islands on both sides of the unit cell, and eventually covers the whole surface. However, even at about 1 ML, there are faint lines along the original positions of the 7×7 unit-cell boundaries, suggesting that the underlying 7×7 structure is undisturbed. This has also been seen for Pb on Si(111).[16]

We can make one other interesting observation about the electronic structure of the surface after RT Ag deposition. Scanning tunneling spectroscopy (STS) curves by Tosch and Neddermeyer[14] show that the surface is semiconducting over the Ag islands, in contrast to the metallic 7×7 surface. Since the states in the band gap are primarily Si adatoms derived on the clean surface, this shows that the Si adatoms are strongly interacting with the adsorbed Ag. What is interesting is that the STS curves for RT adsorption are very similar to the curves for the annealed Ag/Si phases.[18] All of the Ag/Si annealed surface phases are semiconducting.

B. Phase diagram

The production of ordered reconstructions require Ag deposition at elevated substrate temperature, or annealing after deposition. We have studied surface order as a function of the Ag coverage and the annealing conditions using STM as well as LEED. We have found that the experimental conditions for the formation of an ordered phase is dependent on coverage, deposition rate, and thermal annealing history.

Based on STM and LEED observations, we constructed a phase diagram for this system shown in Fig. 2. The small circles and arrows in this figure indicate histories of individual samples, indicating specific preparation conditions after which STM images were taken. The arrows and dashed lines indicate the sequence of measurements for each sample. Note that the lines are shown as vertical, which means that no attempt was made in this diagram to adjust the indicated coverage to account for desorption of Ag at high temperatures. Several sequences for which the initial Ag deposition was at elevated temperatures are also shown. As is apparent from Fig. 2, as far as the mixture of ordered phases on a given sample surface is concerned, there was little difference between a sample that had Ag deposited at RT and then annealed, and a sample that had the same amount of Ag de-

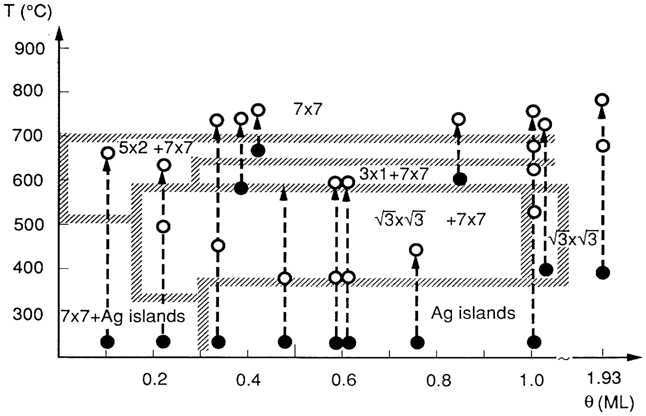

FIG. 2. Phase diagram, showing surface reconstructions vs Ag coverage and annealing or growth temperature. The solid circles indicate initial growth conditions for a given sequence.

posited at an elevated temperature. However, the two sample preparation methods did result in subtle differences such as domain size distributions. These points will be discussed in a following section.

From this diagram, we see the following general features: the most common ordered phase is the $\sqrt{3}\times\sqrt{3}$ phase which is observed at almost any Ag coverage and at 300~550 °C substrate temperature. When the Ag coverage exceeds 1 ML in this temperature range, the entire surface can be covered by the $\sqrt{3}\times\sqrt{3}$ phase. The 3×1 structure appears at higher temperature ($T>550$ °C). Once the temperature exceeds 550 °C, Ag starts to desorb and the $\sqrt{3}\times\sqrt{3}$ phase is gradually converted to the 3×1 phase. When the temperature reaches about 650 °C, a surprising development is revealed: a new surface reconstruction showing a 5×2 periodicity. This new reconstruction was also seen by LEED. This 5×2 structure only exists in the narrow temperature range 650–750 °C and the coverage of Ag is apparently less than that of the 3×1 phase. The 5×2 phase has not been reported previously. Further annealing over 700 °C results in desorption of all Ag, and recovery of the clean Si 7×7 structure. The detailed behavior of each phase will be discussed in the following sections.

C. $\sqrt{3}\times\sqrt{3}$ phase

1. Atomic structure of the $\sqrt{3}\times\sqrt{3}$ phase

Considerable efforts have been made in the structural analysis of the Ag induced $\sqrt{3}\times\sqrt{3}$ phase. There have been a number of recent results that all agree on a structure that is referred to as the honeycomb-chain-trimer (HCT) model.[12] Figure 3 shows this model from the top (upper panel) and in a perspective view (lower panel). This structure is derived from a Si(111) bulk termination by removing the top half of the first bilayer of Si atoms, forming trimers out of the remaining Si atoms, and then adding a full monolayer of Ag atoms in positions slightly distorted from a regular triangular lattice. Electronic structure calculations and simulated STM images based on this model predict[12,19] a honeycomb structure for empty states lying within two volts of the Fermi level which agrees with previously published STM images.[10,11] These calculations also predict that the filled states should show a minimum centered over the Si trimers, and maxima corresponding to the positions of the Ag atoms. To verify these predictions, we investigated the atomic structure of this phase by STM. The STM images have a strong dependence on bias voltage polarity. The empty-states image shows a honeycomb structure with $\frac{2}{3}$ ML of bright dots, with each bright dot corresponding to a position in the center of three Ag atoms, leading to the full monolayer Ag coverage. The filled-states image has three weak maxima corresponding to each bright dot in the empty-state image. The positions of the maxima in the filled-state images agree with actual Ag atom positions in the HCT model. These specific results on the $\sqrt{3}\times\sqrt{3}$ phase have been reported previously.[18]

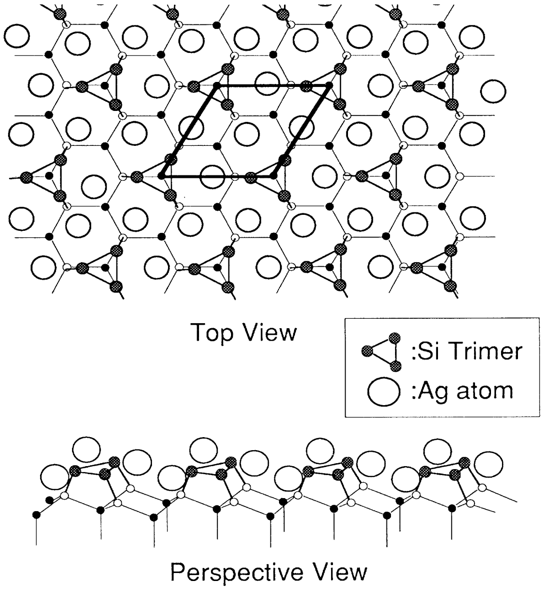

FIG. 3. Honeycomb-chain-trimer model for the $\sqrt{3}\times\sqrt{3}$ phase. Upper panel, a top view, and lower panel, a perspective view.

The determination of the registration between the $\sqrt{3}\times\sqrt{3}$ structure and the underlying Si bulk lattice have been made by examining the registry of the $\sqrt{3}\times\sqrt{3}$ maxima with respect to adatom positions in adjacent areas of the native Si(111) structure. We have found new information about the registration of the $\sqrt{3}\times\sqrt{3}$ surface with respect to the underlying Si(111) lattice. Taking into account the construction of the HCT model, the top Si layer in the $\sqrt{3}\times\sqrt{3}$ surface can be bonded to two threefold symmetric sites on an otherwise unreconstructed Si surface. The two alternatives are the sites having the center of the Si trimer over second layer Si atoms (denoted T_4), or over threefold hollows in the Si double layer (denoted H_3).

The clearest demonstration of the coexistence of these two registrations is at a phase boundary between two inequivalent $\sqrt{3}\times\sqrt{3}$ domains. Figure 4 is an empty-states image containing two domains of the $\sqrt{3}\times\sqrt{3}$ structure separated by a boundary. The boundary appears as a ragged white line and has a zigzag character with straight segments running along the sides of the $\sqrt{3}\times\sqrt{3}$ unit cell, i.e., along $\langle 11\bar{2}\rangle$ directions. The height of the boundary itself is bias dependent as we will discuss in the next section. This image shows that the two domains have the same atomic height, indicating that there is no atomic steps between the two sides. To demonstrate the registration information in this image, Fig. 5(a) shows a portion of the same image with a substrate 1×1 grid superimposed. The grid is aligned in such a way that the holes at the center of the honeycombs in the lower left $\sqrt{3}\times\sqrt{3}$ domain are located at intersections of the grid. When the grid is extended across the boundary to the upper right domain, we find that the registry is shifted. The honeycombs are now centered on upward-pointing triangles. The shift in registry is also shown in the magnified inserts on either side. Figure 5(b) is a diagram that corresponds to the image in Fig. 5(a). A triangular grid defines the Si(111) 1×1 unit cell and the dark triangles denote the Si trimers (which appear as dark holes in the STM image). The positions of the Si trimers over the T_4 and H_3 sites are indicated by open triangles in the insert. The meaning of the shift in registration is apparent in this diagram. If the Si trimers in the lower left domain are assumed to be located over the T_4 site, the sites for the Si trimers in the upper right domain would be over the H_3 site, based on the positions of the dark holes in the STM image. This particular domain boundary was imaged on a sample that was entirely covered by the $\sqrt{3}\times\sqrt{3}$ phase so that it was not possible to determine the actual registration of either side. However, similar measurements at different 7×7-$\sqrt{3}\times\sqrt{3}$ phase boundaries on other samples have confirmed the existence of these two inequivalent registrations.

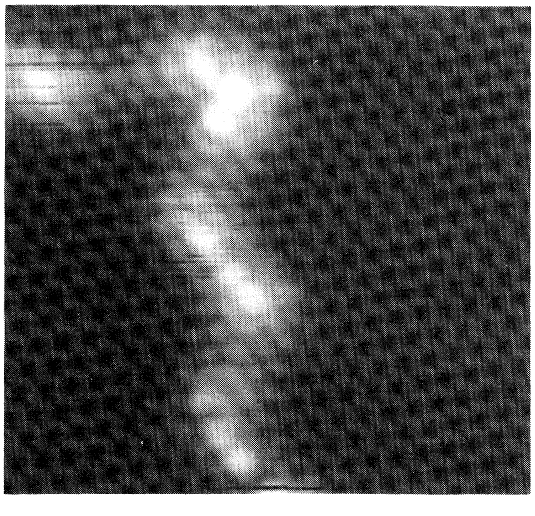

FIG. 4. Empty-states STM image showing two $\sqrt{3}\times\sqrt{3}$ domains separated by a boundary.

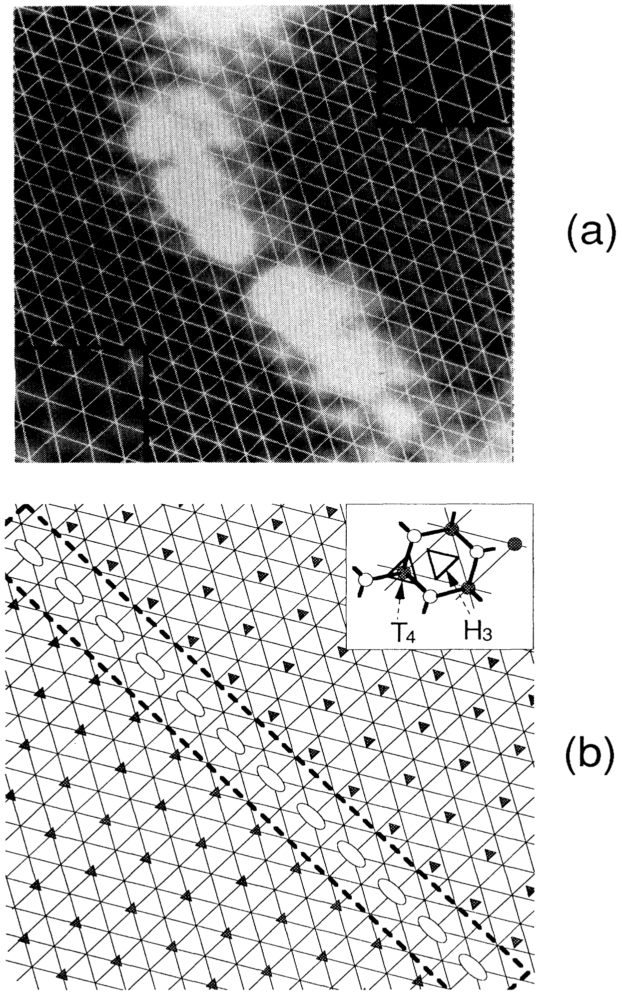

FIG. 5. (a) Portion of the image in Fig. 4 with a superimposed 1×1 grid. (b) Illustration of the shift in the registration of the $\sqrt{3}\times\sqrt{3}$ phase with respect to the grid. Dark triangles denote the positions of the Si trimers in the HCT model. The insert shows the positions of these triangles with respect to the underlying Si bilayer.

The presence of two different registrations has an important effect on the overall structure of the surface because of the particular construction of the HCT model. The inset in Fig. 5(b) shows a 1×1 unit cell of the Si bilayer underlying the $\sqrt{3}\times\sqrt{3}$ phase. The white atoms are those which have dangling bonds available for bonding to the Si trimers. The two triangles represent the two possible sites for the Si trimer. It is apparent that the shift from the T_4 site to the H_3 site results in not only a lateral shift, but it also necessitates a 180° rotation of the Si trimer. Figure 6 shows the two possible configurations for the HCT structure. We assume in this diagram that the behavior of the Ag atoms is basically the same in both cases, so that a rotation of the Si trimers basically rotates the entire top Ag/Si layer. Clearly this will have a major impact on the interpretation of previous data from structural techniques such as ion scattering and

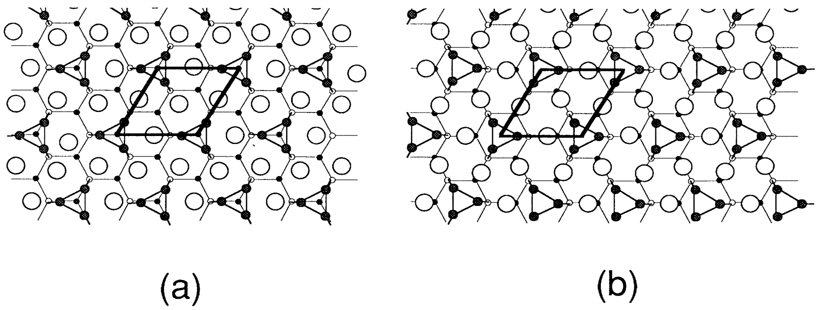

FIG. 6. Schematic drawing of the two registrations of the HCT model for the $\sqrt{3}\times\sqrt{3}$ surface with the Si atoms trimerized on top of T_4 (a) and H_3 (b) sites.

LEED,[3,6] where the results are sensitive to the azimuthal orientation of the surface structure with respect to the bulk crystallographic directions.

The size of individual domains is typically in the range of 200–300 Å for samples at a Ag coverage of 1 ML. This domain size is defined by the average distance seen in large area images between flat boundaries (Fig. 4), as well as between steps. A typical large image is shown in Fig. 7. As can be seen in this image, the step and island density of such a surface is larger than what is expected from the local vicinality of the original clean surface. This domain size is typical of a sample at 1 ML Ag prepared by deposition at elevated temperature. The domains were smaller for samples prepared by annealing RT deposited Ag, but were not below 100 Å in any case.

Unfortunately, it is not possible to determine whether adjacent domains in these large area images are equivalent or not. For practical reasons, we have been able to make detailed registration determinations at only a handful of phase boundaries. This means that it is not possible at this time to make a statement about the relative coverage of the two different registrations. Total energy calculations estimate that the energy difference between the two structures shown in Fig. 6 is very small.[20]

The question arises in the above determination whether the shifts can be due to dislocations of the underlying substrate lattice. We rule out this possibility by the fact that the clean surface does not have any dislocations in very large 7×7 terraces (~1000 Å), and that all the $\sqrt{3}\times\sqrt{3}$ surfaces have finite domain size of about 200 Å. Furthermore, if there were a dislocation of the bulk lattice between two domains, it should be accompanied by a vertical dislocation between two domains, which we did not observe. Thus, we conclude that the $\sqrt{3}\times\sqrt{3}$ phase has two inequivalent registrations to the underlying bulk lattice.

Figure 7 also illustrates the bias-dependent behavior of the domain boundaries in the $\sqrt{3}\times\sqrt{3}$ phase. In the empty-states image [Fig. 7(b)], the boundaries are bright, just as in Fig. 4. However, in the filled states, the same boundaries appear as dips. It is also interesting that step edges between $\sqrt{3}\times\sqrt{3}$ areas also show the same behavior, whereas step boundaries between the $\sqrt{3}\times\sqrt{3}$ and either the 7×7 or the 3×1 do not. A similar bias polarity dependence has been seen for domain boundaries in the Au/Si(111): $\sqrt{3}\times\sqrt{3}$ structure.[21]

2. *Coverage determination*

The question of the Ag coverage in the $\sqrt{3}\times\sqrt{3}$ phase has not been resolved, with different works giving different coverages in the range of $\frac{2}{3}$ to 1 ML. Recently, Raynerd, Hardiman, and Venables[22] showed that the Ag coverage of this phase is temperature dependent: ~1 ML for deposition temperature of 427 °C and $\sim\frac{2}{3}$ ML for 347 °C, which implies that the microstructure of this

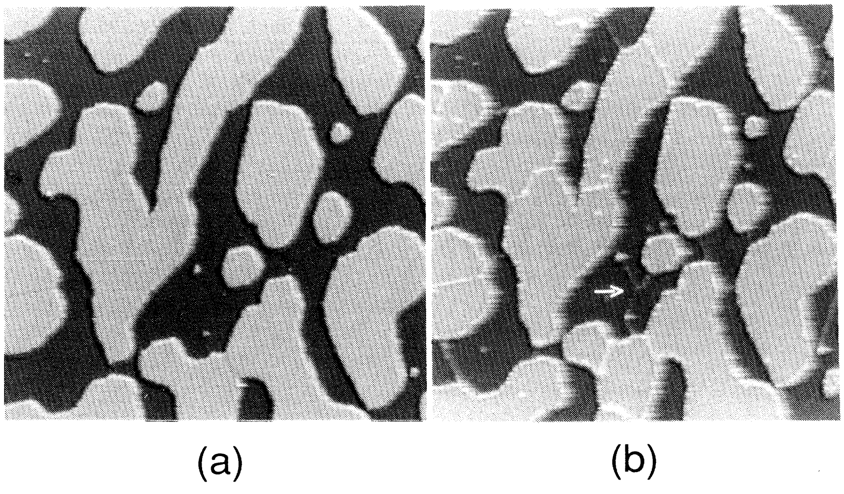

FIG. 7. Large-scale (1300×1500 Å^2) STM images of $\sqrt{3}\times\sqrt{3}$ domains, showing (a) the filled states and (b) the empty states. Both images were taken over the same sample area.

phase can accommodate a range of coverages. On the other hand, the HCT model requires that the Ag coverage of the $\sqrt{3}\times\sqrt{3}$ surface is one monolayer. We can examine the coverage-dependent growth of the $\sqrt{3}\times\sqrt{3}$ phase in order to estimate both the Ag and Si atomic density in the $\sqrt{3}\times\sqrt{3}$ phase.

To determine the Ag coverage, one relies on the fact that the Ag atoms are expected to remain on the surface without desorbing or intermixing when forming the $\sqrt{3}\times\sqrt{3}$ phase. A known amount of Ag (a nominal Ag coverage) is deposited and then annealed until the $\sqrt{3}\times\sqrt{3}$ phase appears. One obtains the fractional coverage of the Ag $\sqrt{3}\times\sqrt{3}$ phase from STM images by simply measuring the $\sqrt{3}\times\sqrt{3}$ concentration with respect to the 7×7. A comparison of the nominal Ag coverage versus the fractional area of the surface covered by the $\sqrt{3}\times\sqrt{3}$ phase would then lead to a measurement of the density of Ag in the $\sqrt{3}\times\sqrt{3}$ phase. We tested this idea by preparing several surfaces of 0.1, 0.3, 0.4, and 0.5 ML nominal Ag coverage while the samples were kept at RT, followed by annealing to about 450 °C. The images obtained from these surfaces consisted of $\sqrt{3}\times\sqrt{3}$ islands as well as clean 7×7 areas. The images show that the fractional coverage of the $\sqrt{3}\times\sqrt{3}$ phase is close to the values of the nominal coverage read by the QCO. Figure 8 shows typical images for Ag deposited on to a 400 °C surface, forming the $\sqrt{3}\times\sqrt{3}$ phase. Panel (a) is an image for 0.48 ML Ag, while panel (b) is an image for 1.05 ML Ag. From these and other images on this sample, the fractions of the surface covered by the $\sqrt{3}\times\sqrt{3}$ phase at the two coverages were 0.5 and 1.0 ML, respectively. Thus, we believe that the Ag coverage necessary to form the $\sqrt{3}\times\sqrt{3}$ phase is approximately 1 ML.

This estimation relies on the absolute accuracy of the Ag coverage and the Ag evaporation calibration. From our experience in other metal and Si systems with exactly the same apparatus, we estimate that our absolute coverages are certainly within 20% of the nominal figure in the worst case. We believe that this accuracy is sufficient to exclude $\frac{2}{3}$ ML as a realistic Ag density for the $\sqrt{3}\times\sqrt{3}$ phase. Furthermore, we do not see any change in the estimated Ag density for $\sqrt{3}\times\sqrt{3}$ surfaces grown at substrate temperatures as low as 400 °C as shown in Fig. 8.

Another aspect of the geometric structure is the conservation of the silicon atoms in the transformation from the clean 7×7 structure to the $\sqrt{3}\times\sqrt{3}$ structure. In the HCT model, the top half of a Si bilayer is missing, leaving a density of Si atoms in the $\sqrt{3}\times\sqrt{3}$ phase of one monolayer. Using STM measurements, it is possible to estimate the density change of silicon atoms in the reconstructed layers through the transformation from the original 7×7. From Figs. 7 and 8, we see that the $\sqrt{3}\times\sqrt{3}$ islands appear not only above the original surface level, but also are embedded in the surface. The boundaries of the $\sqrt{3}\times\sqrt{3}$ areas are very irregular as are the steps between different $\sqrt{3}\times\sqrt{3}$ terraces. Consider the growth of the $\sqrt{3}\times\sqrt{3}$ phase starting from a flat 7×7 Si(111) terrace illustrated in Figs. 9(a) and 9(b), which shows a $\sqrt{3}\times\sqrt{3}$ island with area S_1 produced by Ag deposition. The excess Si atoms that were removed to form the $\sqrt{3}\times\sqrt{3}$ area accumulate to form a 7×7 island one bilayer step higher than the original terrace (area S_2). The density of silicon atoms in the $\sqrt{3}\times\sqrt{3}$ layers, $N_{\sqrt{3}\times\sqrt{3}}$, can be obtained from the measurement of the area ratio S_2/S_1, independent of the coverage of silver, by the relation

$$N_{\sqrt{3}\times\sqrt{3}}S_1+N_7S_2+2S_2=N_7(S_1+S_2)\ ,$$

where N_7 is the density of silicon atoms in the 7×7 reconstructed surface and $2S_2$ accounts for the additional Si atoms needed to raise S_2 by a bilayer step. This process can be understood by the surface energies of both $\sqrt{3}\times\sqrt{3}$ and 7×7 phases. Theoretical calculations[12] predict that the HCT model of the $\sqrt{3}\times\sqrt{3}$ phase has a lower surface energy than the 7×7. One would expect that both phases can compete each other to form stable structures. Our picture of the growth of Ag on Si(111) is as follows: after the Ag atoms begin to form the $\sqrt{3}\times\sqrt{3}$ phase and replace the top layer Si atoms, the

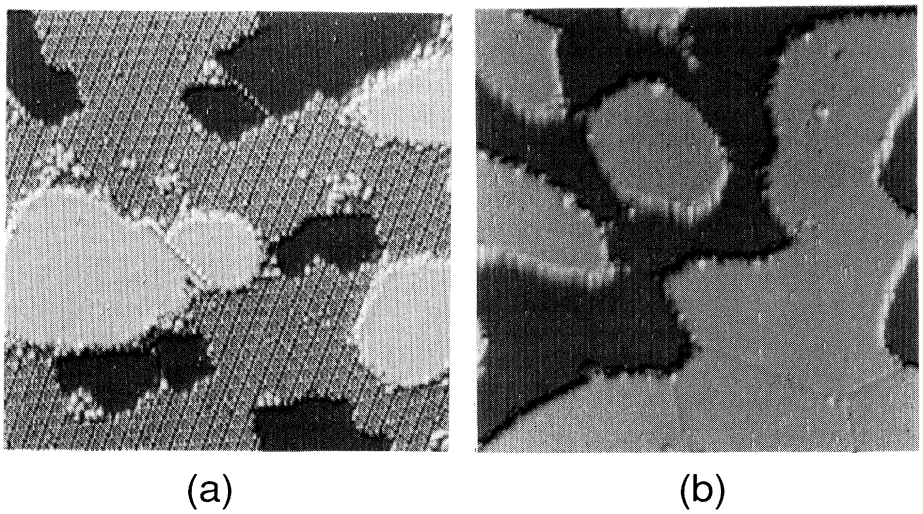

FIG. 8. Ag/Si(111)-$\sqrt{3}\times\sqrt{3}$ surfaces produced at (a) 0.48 ML; (b) 1.05 ML at 400 °C.

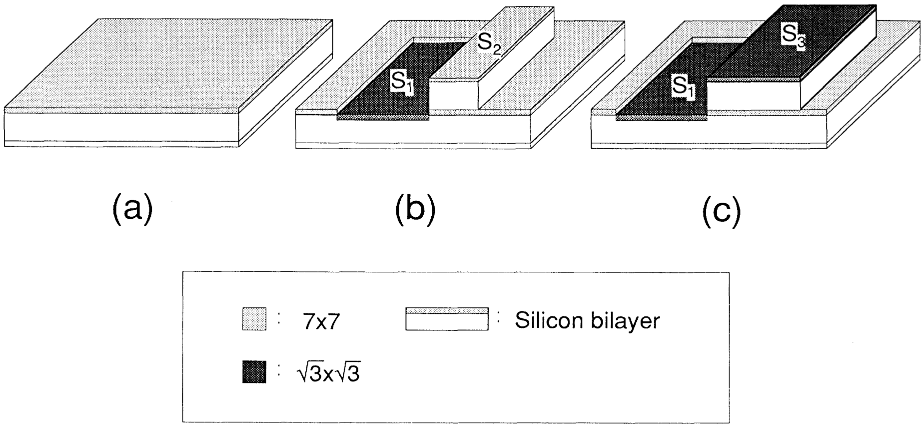

FIG. 9. Schematic of the growth of a $\sqrt{3}\times\sqrt{3}$ area on the 7×7 surface. (a) A flat 7×7 surface. (b) An area (S_1) of the $\sqrt{3}\times\sqrt{3}$ phase and a raised terrace (S_2) of displaced Si. (c) The entire surface covered by the $\sqrt{3}\times\sqrt{3}$ phase.

excess Ag atoms and the Si atoms then coalesce to form their own ordered structures: $\sqrt{3}\times\sqrt{3}$ for Ag atoms, and 7×7 for surplus Si atoms.

The actual situation when 7×7 and $\sqrt{3}\times\sqrt{3}$ phases coexist is one step more complicated than is represented by Figs. 9(a) and 9(b). The most common growth mode is the formation of adjacent holes and raised island, both terminated in the $\sqrt{3}\times\sqrt{3}$ phase, as seen in Figs. 8(a) and 9(c). Using conservation of Si, we have the following relationship between the area of embedded $\sqrt{3}\times\sqrt{3}$ (S_1) and the raised $\sqrt{3}\times\sqrt{3}$ (S_3):

$$N_{\sqrt{3}\times\sqrt{3}}S_1+N_{\sqrt{3}\times\sqrt{3}}S_3+2S_3=N_7(S_1+S_3)$$

or

$$N_{\sqrt{3}\times\sqrt{3}}=N_7-2S_3/(S_1+S_3)\ .$$

Assuming the Takayanagi model for the 7×7 surface,[23] $N_7=2.08$ atoms per 1×1 unit cell. The area ratio S_3/S_1 can be easily measured by the STM images for different mixes $7\times7/\sqrt{3}\times\sqrt{3}$ surfaces. Thus, $N_{\sqrt{3}\times\sqrt{3}}$ can be estimated by the above equation. Figure 10 shows measurements for different experimental runs (different Ag coverages) with each point representing averages over several images in different areas of a given sample. It should be noted that the ratio S_3/S_1 is independent of substrate temperature and Ag coverage. The value of S_3/S_1 is approximately unity which gives a value of approximately one for $N_{\sqrt{3}\times\sqrt{3}}$ in the above equation. This is consistent with a value for Si density of 1 ML determined by the reflection electron microscopy study,[9] where it was found that the surplus silicon atoms produced at the central part of wide terraces form two-dimensional islands. This value is also consistent with the HCT model.

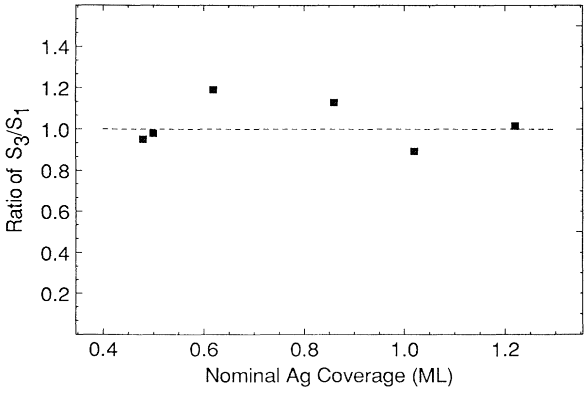

FIG. 10. Ratio of S_3/S_1 as a function of the nominal Ag coverage.

D. 3×1 phase

To prepare the 3×1 structure, we can start from the $\sqrt{3}\times\sqrt{3}$ surface, produced at any coverage as described previously, and then anneal it for several minutes at about 600 °C. Temperatures above 550 °C are sufficient to desorb Ag from the surface. LEED shows a gradual evolution of a strong 3×1 pattern with some streaks in $\langle 1\bar{1}0\rangle$ directions, and with some intensity in $\sqrt{3}\times\sqrt{3}$ positions still present. The LEED pattern changes to 6×1 at room temperature. We will continue to refer to the RT 6×1 structure as 3×1 for the remainder of this paper.

Figure 11 presents the evolution of a surface starting from a $\sqrt{3}\times\sqrt{3}$ phase with annealing temperatures up to 650 °C. After annealing the surface to about 600 °C, we observe the coexistence of three types of structures: 7×7, $\sqrt{3}\times\sqrt{3}$, and 3×1 as shown in panel (a). Panel (b) is a diagram to label the areas of these three structures. First, we note that the 3×1 structure consists of rows running along $\langle 1\bar{1}0\rangle$ directions (too fine to be seen at this magnification), and that boundaries between the 7×7 and 3×1 phases also run also these directions, as do the boundaries between 3×1 and $\sqrt{3}\times\sqrt{3}$. Second, there are very few adjacent areas of 7×7 and $\sqrt{3}\times\sqrt{3}$ on samples where the 7×7 has been uncovered through Ag desorption. The $\sqrt{3}\times\sqrt{3}$ and 7×7 phases are separated by areas of 3×1, except in a few instances with small islands of remaining $\sqrt{3}\times\sqrt{3}$ that are separated from the 7×7 by a step edge. This reflects the fact that the Ag content of the 3×1 phase is intermediate to that of the $\sqrt{3}\times\sqrt{3}$ and the 7×7. Furthermore, it has not been

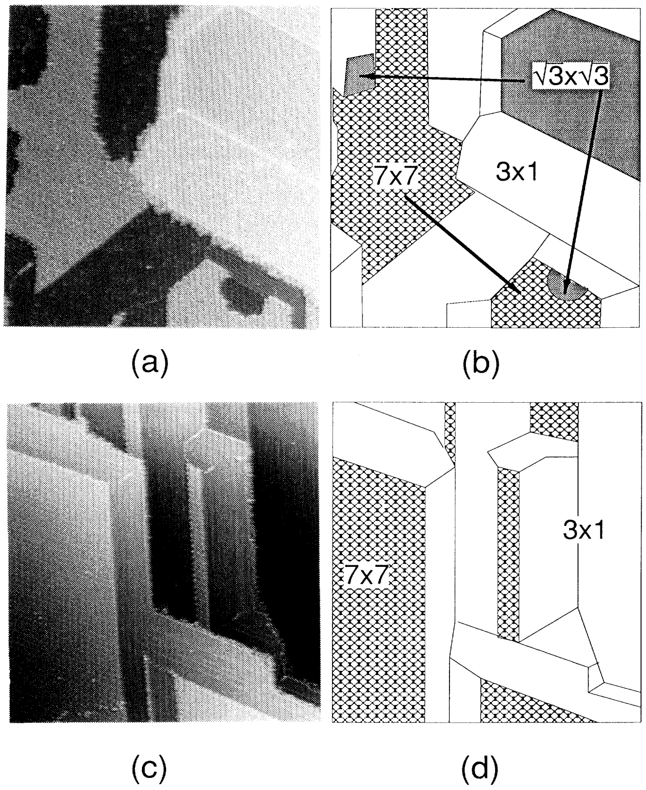

FIG. 11. Transformation of the $\sqrt{3}\times\sqrt{3}$ phase to the 3×1 phase upon annealing. (a) Coexistence of the $\sqrt{3}\times\sqrt{3}$, the 3×1, and the 7×7 phases after 600 °C annealing. (c) The surface after annealing to 650 °C. (b) and (d) are diagrams showing the areas of each phase in (a) and (c).

possible to produce a sample by desorption having only $\sqrt{3}\times\sqrt{3}$ and 3×1 without any 7×7.

After the annealing temperature is increased to 650 °C, the $\sqrt{3}\times\sqrt{3}$ phase entirely converts to a 3×1 phase, leaving only 3×1 and 7×7 on the surface as shown in panel (c). Panel (d) labels the areas of 3×1 and 7×7. We also note that the overall fractional area of the surface covered by the 3×1 phase is increased compared to the original fraction of the $\sqrt{3}\times\sqrt{3}$ phase on this sample, which further supports the fact that the Ag coverage of the 3×1 phase is lower than that of the $\sqrt{3}\times\sqrt{3}$ phase.

The 3×1 surface can also be produced directly from the clean 7×7 surface without passing through the $\sqrt{3}\times\sqrt{3}$ phase. This is done by depositing some amount of Ag (<1 ML), while the sample is held at about 600 °C. The difference with this preparation is that the 3×1 phase is nucleated at step edges of the clean 7×7 surface and there is a strong tendency for the 3×1 rows to extend from the lower side of a step edge. It is possible to produce large domains of the 3×1 phase in this manner, as large as several hundreds of Å, since the starting surface has not had its step and terrace structure disturbed by the formation of the $\sqrt{3}\times\sqrt{3}$ phase. But, unlike the $\sqrt{3}\times\sqrt{3}$ phase, the 3×1 phase never covers the entire surface and it always coexists with 7×7 phase. If more than 1 ML of Ag is deposited on a 600 °C surface, we start to observe $\sqrt{3}\times\sqrt{3}$ LEED spots coexisting with the 3×1 and 7×7 patterns. If the substrate temperature is lowered to 550 °C or below, then a $\sqrt{3}\times\sqrt{3}/7\times7$ surface is grown, with no 3×1 phase. Thus the formation of the 3×1 phase is in a relatively small area of the phase diagram.

A recent low-energy electron microscopy (LEEM) study by Denier van der Gon and Tromp gives some additional insight into the formation of the 3×1 and $\sqrt{3}\times\sqrt{3}$ phases.[24] They demonstrate that when Ag is deposited at a substrate temperature of 885 K, the 7×7 surface is gradually converted to 3×1. This conversion is a function of terrace width: narrower terraces of 7×7 can be converted entirely to the 3×1 phase and then start to be converted to $\sqrt{3}\times\sqrt{3}$ at the same coverage at which wider terraces have not completed the conversion from 7×7 to 3×1. This accounts for the coexistence of all three phases in our high-temperature depositions. If the Ag flux is turned off at 885 K in the LEEM experiment, Ag starts to desorb and the $\sqrt{3}\times\sqrt{3}$ surface is seen to convert entirely to the 3×1 phase before the appearance of the 7×7. Our inability to observe the 3×1 without the 7×7 after desorption reflects the fact that the desorption is too rapid for us to be able to arrest the process at a point before the Ag coverage has dropped to below that of the 3×1 phase.

The detailed structure of the 3×1 phase is shown in Fig. 12. Figure 12 is a dual bias image taken at $V_S=1$ V for empty states [Fig. 12(a)] and $V_S=-1$ V for filled states [Fig. 12(b)]. These images were taken in parallel in order to retain their spatial registration. This registration was checked independently by comparing the positions of adatoms in an adjacent area of 7×7 in the same image that was trimmed from this figure. The empty states show a well-defined 3×1 periodicity with bright rows running along $\langle 1\bar{1}0\rangle$ directions, spaced three 1×1 unit cells apart. To either side of each bright row are small protrusions, spaced at a $1a$ spacing along the row, and roughly pointed in $\langle 11\bar{2}\rangle$ type directions ($a=a_0/\sqrt{3}=3.84$ Å).

Similar to the $\sqrt{3}\times\sqrt{3}$ phase, the 3×1 features seen in Fig. 12 appear significantly different depending on the bias voltage polarity. The rows in filled-state images appear like flat stripes, once again spaced $3a$ apart. However, the filled states show a clear 6×1 rather than 3×1 periodicity since the $1a$ periodicity along each row is different in adjacent rows. The correspondence between the maxima positions in both empty and filled states are indicated by the 3×1 unit-cell outline marked in the same position in both images. We see that the position of central bright line in the empty states corresponds to the center of the stripes in the filled states. Inside the 3×1 unit cell, the maxima in the filled states are located at the trough between the shoulder maxima in empty states.

Before we propose a possible atomic structure of the 3×1 phase, we will show the morphology and registration of the 3×1 subunits. We first discuss the vertical height of the 3×1 surface, which is a very important issue in determining the registration of the 3×1 phase. Since we have already studied the bias dependence of

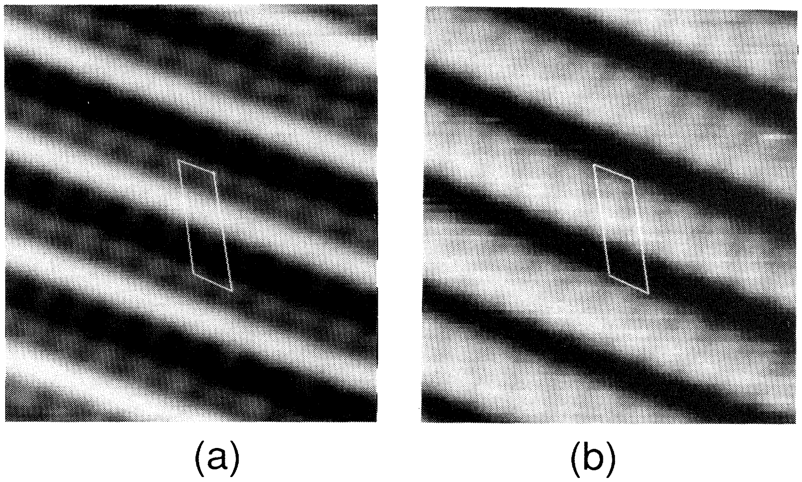

FIG. 12. Dual bias images of the 3×1 phase showing (a) empty states and (b) filled states. A single 3×1 unit cell is marked in equivalent positions in both images.

7×7-$\sqrt{3}\times\sqrt{3}$ boundaries,[18] it is useful to compare the vertical heights of both the 3×1 and the $\sqrt{3}\times\sqrt{3}$ phases with the adjacent 7×7 phase. Figure 13(a) is an empty-states image taken on a sample such as shown in Fig. 11(a), where the three phases coexist. The 7×7, 3×1, and $\sqrt{3}\times\sqrt{3}$ phases are marked and characterized by adatoms, rows, and honeycomb patterns, respectively. The heights of both 3×1 and $\sqrt{3}\times\sqrt{3}$ phases are approximately the same as illustrated in Fig. 13(b), which shows the cross section along the white line in Fig. 13(a). Furthermore, we find that the bias voltage dependence of a $7\times7/3\times1$ step is similar to that of a 7×7-$\sqrt{3}\times\sqrt{3}$ step, and that the STS curves of the $\sqrt{3}\times\sqrt{3}$ and the 3×1 phase are similar. Thus, we expect the surface profile in Fig. 13(b) to correspond to the schematic structure shown in Fig. 14. The 7×7-$\sqrt{3}\times\sqrt{3}$ step geometry is consistent with the bias voltage dependence from our previous study. The fact that the 3×1 and the $\sqrt{3}\times\sqrt{3}$ phase are at the same height strongly implies that the 3×1 phase is built up on top of the Si bilayer that is one step below the adjacent 7×7 area, and the relatively large height of the 3×1 above this bilayer suggests that it is a "missing top layer" structure similar to the $\sqrt{3}\times\sqrt{3}$ phase.

We now examine the registration of the 3×1 structure with respect to the 7×7 reconstruction, thereby determining the location of the features in the 3×1 STM image. Figure 15 is an empty-states image with an area of the 3×1 phase surrounded by the 7×7 structure with a grid of 7×7 unit-cell boundaries superimposed. Taking into account the step height information of Fig. 14 and the bias dependence of the 3×1 phase, we construct a diagram to illustrate the 3×1 registration in Fig. 16. A reference bilayer of the bulk Si(111) lattice below the

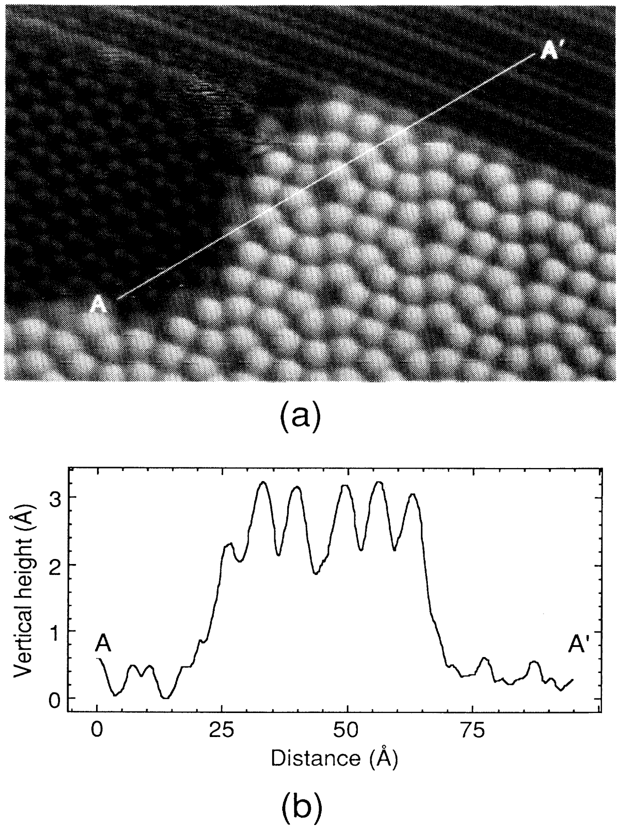

FIG. 13. (a) Image of a mixed 7×7, $\sqrt{3}\times\sqrt{3}$, and 3×1 area. (b) Surface height along the white line marked in (a).

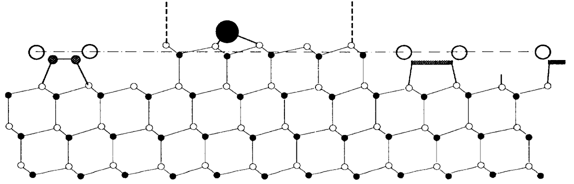

FIG. 14. Schematic view of the step heights at the boundaries between the three phases.

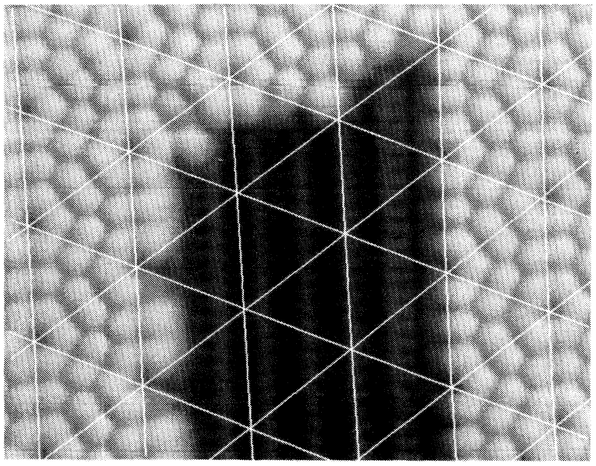

FIG. 15. Empty-states image of the 3×1 phase surrounded by adjacent 7×7 areas with a 7×7 grid superimposed.

3×1 phase is drawn as small circles and the 7×7 adatoms in the surrounding area are denoted as large dark circles. Since the 7×7 areas are one step higher than the reference plane, the 7×7 adatoms lie over H_3-like sites of the reference plane. A triangular grid marks the positions of unit-cell boundaries in the 7×7 structure. The empty electronic states of the 3×1 subunits are shown by unshaded rows and branches. The central ridges in Fig. 16 lie slightly offset from H_3 sites, assuming that the layer directly beneath the 3×1 phase is not reconstructed. The positions of the filled-states features are also shown as shaded ovals. The maxima in the filled states are all located approximately over the T_4 site of the reference plane. Although the strong bias dependence of the images makes it impossible to assign individual features to either Ag or Si atoms, this registration information can serve as a guide for possible atomic models for the 3×1 phase.

Taking into account the information provided by the step height, the registration, and the polarity dependence of the STM images, we propose the structural model shown in Fig. 17. The upper panel is a top view and the lower panel is a side view. In this model, $\frac{2}{3}$ ML of Si atoms form chains on top of a Si(111) bulk terminated surface with an interchain spacing of $3a$. The chains are analogous to the fivefold rings in the π-bonded chain model of the Si(111) 2×1 surface.[25] However, the $3a$ interchain spacing results in an additional $\frac{1}{3}$ ML of "rest atoms" with dangling bonds between the chains. The Ag layer is formed on top of these Si chains with one Ag atom bonding to each dangling bond along the Si chains. There may also be some interaction between Ag-Ag neighbors along each chain.

The primary motivation behind this particular model was to find a structure that was analogous to the HCT model of the $\sqrt{3}\times\sqrt{3}$ phase. The fact that it is a missing top layer model explains the step height information. The local bonding of the Ag atoms is also similar to the $\sqrt{3}\times\sqrt{3}$ phase, with each Ag atom bonding to one Si

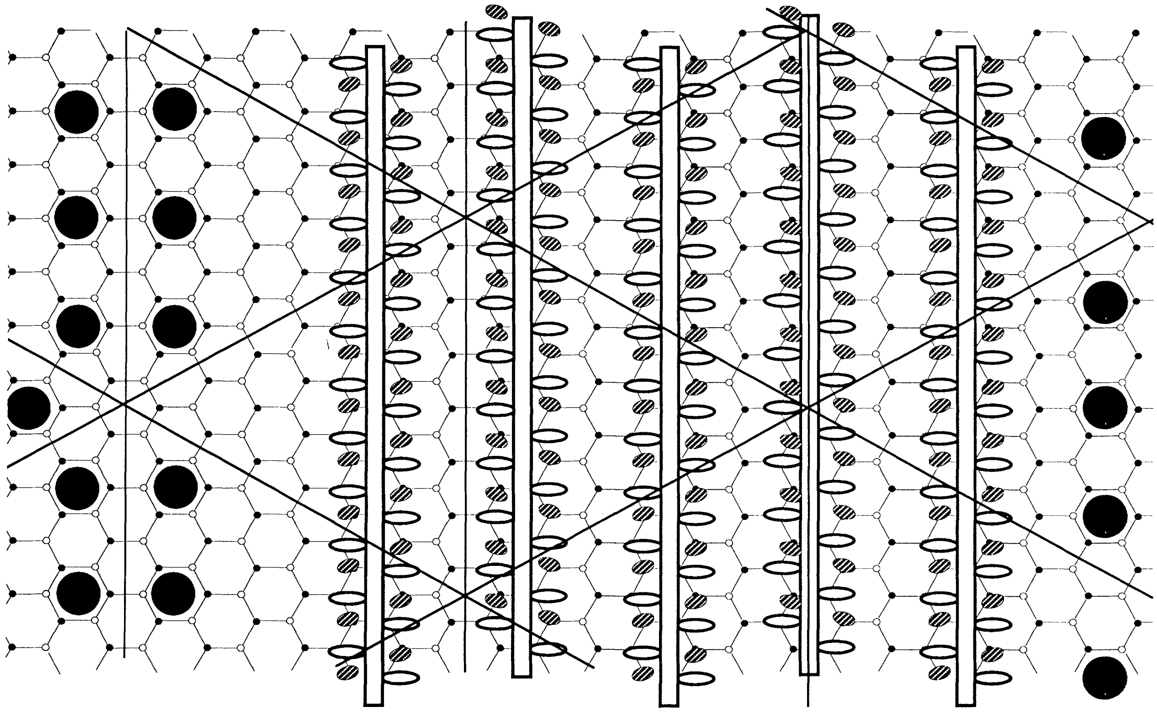

FIG. 16. Drawing showing the positions of filled-state (shaded ovals) and empty-state (unshaded rows and branches) maxima for the 3×1 area shown in Fig. 15.

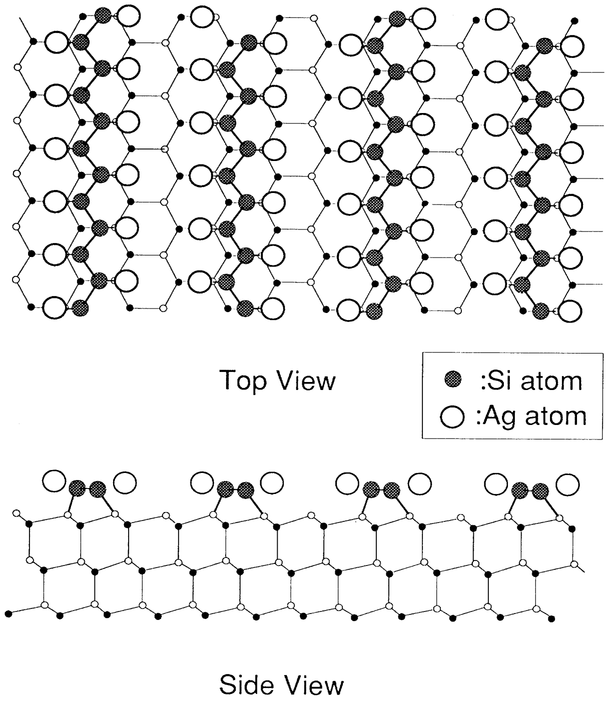

FIG. 17. Proposed model for the Ag/Si(111) 3×1 phase. Upper panel, top view, and lower panel, side view.

dangling bond, while at the same time having two Ag neighbors at a distance of approximately $1a$. The polarity dependence of the STM images also can be understood in analogy to the $\sqrt{3}\times\sqrt{3}$ phase. In the filled states, the $\frac{2}{3}$ ML of maxima that make up the "flat rows" in Fig. 12(b) would correspond more or less to the positions of Ag atoms. The empty-state maxima corresponding to this model are not obvious, but the positions of the centers of each row agree with the registration information in Fig. 16. The appearance of the 6×1 periodicity is not clear but it could be attributed to small displacements of alternate Ag rows along the row direction due to the interactions between the chain. The model of Fig. 17 needs to be investigated by further theoretical and experimental studies.

One possible objection to this particular model is that it requires a Ag density of $\frac{2}{3}$ ML, which does not agree with previous work that has often assumed a coverage of $\frac{1}{3}$ ML.[1,10] In our growth studies, we have not been able to assign a specific Ag coverage to the 3×1 phase since it is formed at substrate temperatures at which Ag is being desorbed. However, we note that the nucleation of $\sqrt{3}\times\sqrt{3}$ on the 3×1 surface as seen by LEEM (Ref. 24) is correlated with a transition in the saturation coverage of Ag on the surface which has been assigned to between 0.6 and 0.7 ML by Raynerd, Hardiman, and Venables.[22] This is consistent with a $\frac{2}{3}$ ML mode for the 3×1 phase.

E. 5×2 phase

The 5×2 phase can be produced either by RT Ag deposition followed by thermal annealing or by hot sample deposition. In either case, the substrate temperature must be between 600 °C and 750 °C depending on Ag coverage and annealing time. After RT deposition, the sequence of ordered phases with annealing is $\sqrt{3}\times\sqrt{3}$, 3×1, and then 5×2. Thus, the Ag coverage of this 5×2 phase should be lower than that of the 3×1 phase. It should also be noted that the 5×2 phase can be grown only in a very narrow range of temperature and coverage near the 3×1 phase. Transformation from 3×1 to 5×2 requires only a slight annealing.

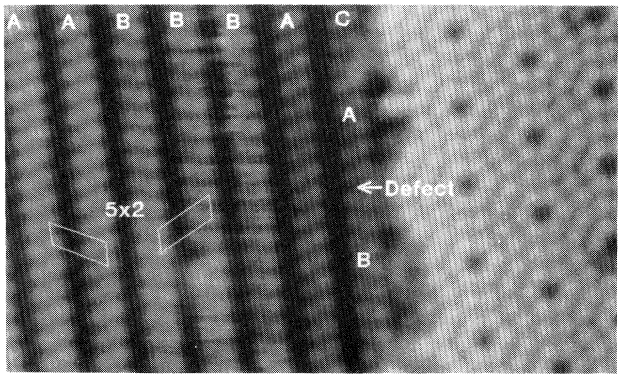

FIG. 18. Empty-state image showing both the 5×2 phase and the 7×7 structure. Rows with the two different orientations for the 5×2 unit cell (white outlines) are labeled "*A*" and "*B*."

LEED observation indicates the presence of $5\times$ periodicity diffraction spots after annealing to 650 °C. The patterns always show a mixture of 7×7 and $5\times$ structure. STM imaging clearly shows the well-ordered regions of 5×2. Figure 18 is an empty-state image which shows an area of 5×2 adjacent to a 7×7 area. The 5×2 phase consists of rows oriented along a $\langle 1\bar{1}0\rangle$ direction and with a 5 unit-cell inter-row spacing. Pairs of protrusions along each row are separated by $2a$, leading to a 5×2 periodicity. It is clear in this image that there are two slightly different local subunits that make up the 5×2 phase. This can be seen by comparing the rows labeled "*A*" with the adjacent ones labeled "*B*." The pairs

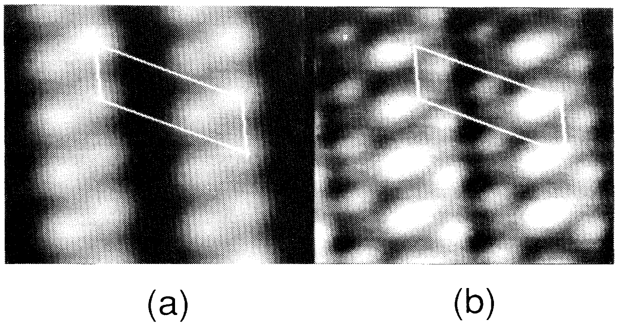
(a) (b)

FIG. 19. Dual bias images of the 5×2 phase, taken in parallel at $+1.5$ V and -1.5 V sample bias, showing the (a) empty and (b) filled states of the surface. The 5×2 unit cell indicates equivalent positions of both images.

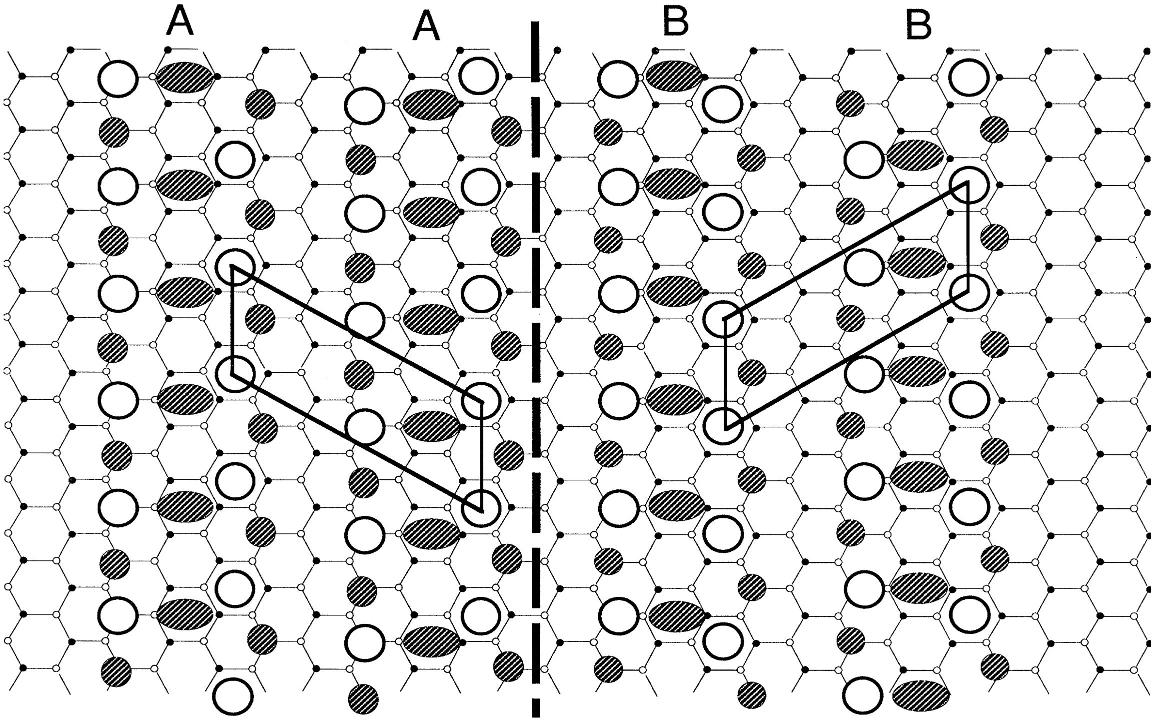

FIG. 20. Line drawing illustrating the correspondence of maxima between the filled states (shaded) and empty stats (unshaded) for the 5×2 phase.

of protrusions making up each of these rows change orientation in going from type "*A*" to type "*B*." This leads to two possible orientations of the 5×2 unit cell. Two 5×2 unit cells are drawn in areas made up of two adjacent type "*A*" or type "*B*" rows. The difference between these two structures must be relatively minor, as row "*C*" is seen to switch between type "*A*" and type "*B*" at a defect.

The appearance of the 5×2 structure in STM images also has a strong dependence on bias voltage polarity. Figure 19 shows a portion of a dual-bias image of the same surface. Once again, the two images were taken in parallel in order to retain their spatial registration. In the empty-states image [Fig. 19(a)], every row consists of maxima which are paired up to form subunits spaced $2a$ along the row. The filled-state image [Fig. 19(b)] is entirely different: the trough between the bright rows shows $2a$ periodicity. The arrangement of the bright features within each row is complicated, but well ordered. The 5×2 unit-cell outline in both biases are over equivalent positions.

We illustrate the registration and approximate spatial extent of the empty and filled electronic states of the 5×2 overlayer features in Fig. 20. The empty-states maxima of the bright features are represented by light-shaded circles and the filled-states maxima are illustrated by dark circles and a set of ovals. This figure shows the two possible orientations of the 5×2 unit cell. It is not possible to associate these maxima with atoms because of the extreme difference of the features seen in the two bias polarities. The 1×1 bilayer is drawn as a reference, but in this case it does not indicate the registration of the 5×2 with the bulk Si lattice. This figure only serves to demonstrate the correspondence of maxima observed between the filled-states and empty-states images. It is not possible to suggest a model for the 5×2 phase, partially because we were not able to extract reliable registration information at the 5×2 and 7×7 phase boundaries.

IV. SUMMARY

In summary, we have studied the growth and ordering behavior of Ag on the Si(111) surface. The STM results reveal that a variety of surface reconstructions occur by changing the Ag coverage and the annealing or growth temperature. The $\sqrt{3}\times\sqrt{3}$ reconstruction is the most stable phase and its STM images are consistent with the theoretical calculations based on the HCT model. Registration information for the HCT model is shown. The growth behavior of the $\sqrt{3}\times\sqrt{3}$ phase is also discussed, in terms of the estimated density of Ag and Si atoms associated with the HCT structure. As the annealing temperature is increased above 550 °C, the $\sqrt{3}\times\sqrt{3}$ phase undergoes a structural transformation to the 3×1 reconstruction. The empty-state images of this 3×1 phase show rows with a clear 3×1 periodicity, whereas the filled-states image reveals an alternation between adjacent rows, giving a 6×1 periodicity. An atomic model for this phase is proposed on the basis of the bias-dependent images and measured registration information. For substrates annealed above 650 °C, a reconstruction characterized by a 5×2 periodicity was observed. Images of the

5×2 reconstruction are also polarity dependent. Diagrams of the positions of the maxima in the 5×2 phase are provided to assist in modeling this new surface structure.

ACKNOWLEDGMENT

X. F. Lin was partially supported by the Graduate School at the University of Wisconsin–Milwaukee.

---

*Author to whom correspondence should be addressed.

[1] See G. LeLay, Surf. Sci. **132**, 169 (1983), and references listed therein.

[2] E. Vlieg, A. W. Denier van der Gon, J. F. van der Veen, J. E. MacDonald, and C. Norris, Surf. Sci. **209**, 100 (1989).

[3] W. C. Fan, A. Ignatiev, H. Huang, and S. Y. Tong, Phys. Rev. Lett. **62**, 403 (1989).

[4] A. Ichimiya, S. Kohmoto, T. Fujii, and Y. Horio, Appl. Surf. Sci. **41/42**, 82 (1989).

[5] E. L. Bullock, G. S. Herman, M. Yamada, D. J. Friedman, and C. S. Fadley, Phys. Rev. B **41**, 1703 (1990).

[6] M. Katayama, R. S. Williams, M. Kato, E. Nomura, and M. Aono, Phys. Rev. Lett. **66**, 2762 (1991).

[7] E. Vlieg, E. Fontes, and J. R. Patel, Phys. Rev. B **43**, 7185 (1991).

[8] T. Takahashi, S. Nakatani, N. Okamoto, T. Ishikawa, and S. Kikuta, Jpn. J. Appl. Phys. **27**, L753 (1988).

[9] Y. Tanishiro, K. Takayanagi, and K. Yagi, Surf. Sci. **258**, L687 (1991).

[10] R. J. Wilson and S. Chiang, Phys. Rev. Lett. **58**, 369 (1987); **59**, 2329 (1987); J. Vac. Sci. Technol. A **6**, 398 (1988).

[11] E. J. van Loenen, J. E. Demuth, R. M. Tromp, and R. J. Hamers, Phys. Rev. Lett. **58**, 373 (1987); J. E. Demuth, E. J. van Loenen, R. M. Tromp, and R. J. Hamers, J. Vac. Sci. Technol. B **6**, 18 (1988).

[12] Y. G. Ding, C. T. Chan, and K. M. Ho, Phys. Rev. Lett. **67**, 1454 (1991), and references listed therein.

[13] Omicron Vakuumphysik Gmbh, Germany.

[14] S. Tosch and H. Neddermeyer, Phys. Rev. Lett. **61**, 349 (1988).

[15] J. Nogami, S. Park, and C. F. Quate, J. Vac. Sci. Technol. B **6**, (4), 1479 (1988).

[16] E. Ganz, I. S. Hwang, F. Xiong, S. K. Theiss, and J. Golovchenko, Surf. Sci. **257**, 259 (1991).

[17] U. K. Kohler, J. E. Demuth, and R. J. Hamers, Phys. Rev. Lett. **60**, 2499 (1988).

[18] K. J. Wan, X. F. Lin, and J. Nogami, Phys. Rev. B **45**, 9509 (1992).

[19] S. Watanabe, M. Aono, M. Tsukada, Phys. Rev. B **44**, 8330 (1991).

[20] K. M. Ho (private communication).

[21] J. Nogami, A. A. Baski, and C. F. Quate, Phys. Rev. Lett. **65**, 1611 (1990).

[22] G. Raynerd, M. Hardiman, and J. A. Venables, Phys. Rev. B **44**, 13 803 (1991).

[23] K. Takayanagi, Y. Tanishiro, M. Takahashi, and S. Takahashi, J. Vac. Sci. Technol. A **3**, 1502 (1985).

[24] A. W. Denier van der Gon and R. M. Tromp, Phys. Rev. Lett. **69**, 3519 (1992).

[25] K. C. Pandey, Phys. Rev. Lett. **47**, 1913 (1981).

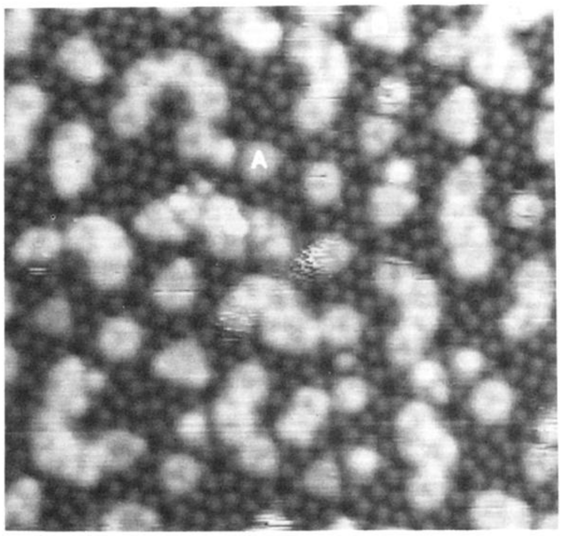

FIG. 1. Empty-state image of 0.5 ML Ag on Si(111) 7×7, deposited at room temperature. Two types of islands are labeled "*A*" and "*B*."

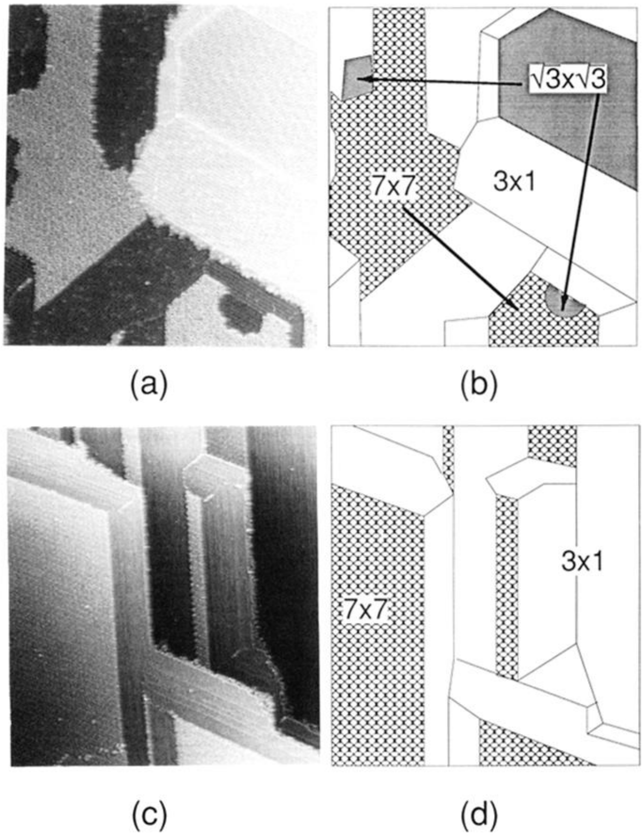

(a) (b)

(c) (d)

FIG. 11. Transformation of the $\sqrt{3}\times\sqrt{3}$ phase to the 3×1 phase upon annealing. (a) Coexistence of the $\sqrt{3}\times\sqrt{3}$, the 3×1, and the 7×7 phases after 600 °C annealing. (c) The surface after annealing to 650 °C. (b) and (d) are diagrams showing the areas of each phase in (a) and (c).

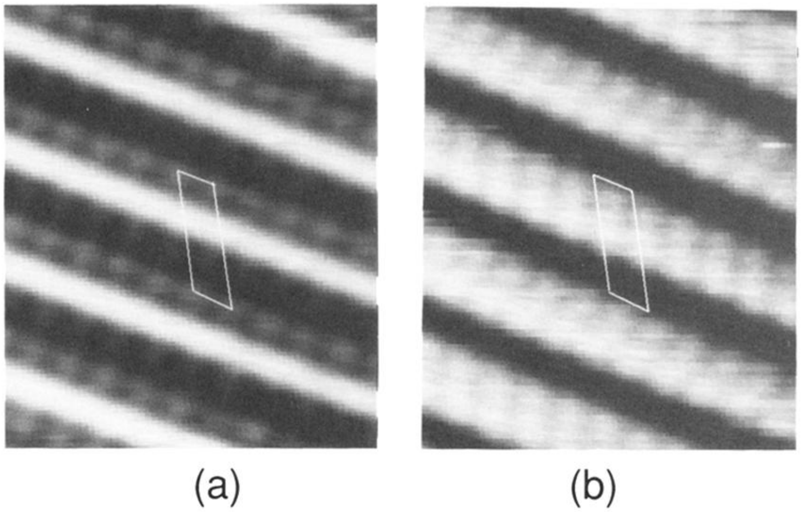

FIG. 12. Dual bias images of the 3×1 phase showing (a) empty states and (b) filled states. A single 3×1 unit cell is marked in equivalent positions in both images.

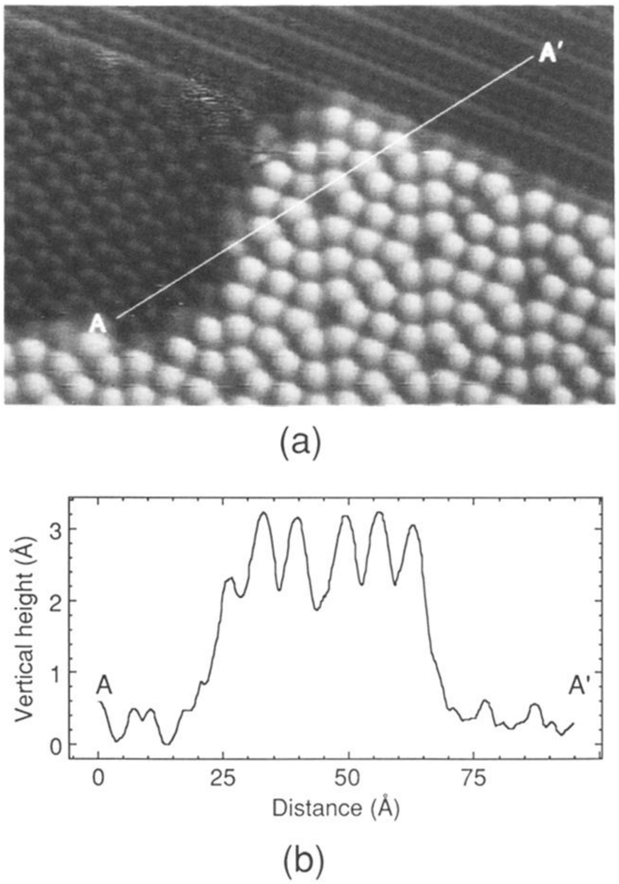

FIG. 13. (a) Image of a mixed 7×7, $\sqrt{3}\times\sqrt{3}$, and 3×1 area. (b) Surface height along the white line marked in (a).

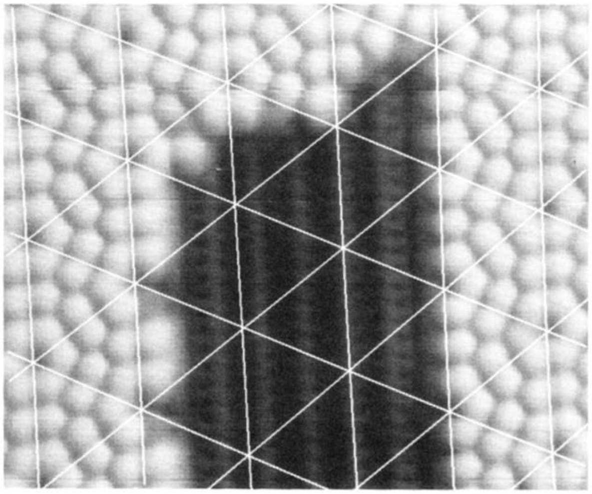

FIG. 15. Empty-states image of the 3×1 phase surrounded by adjacent 7×7 areas with a 7×7 grid superimposed.

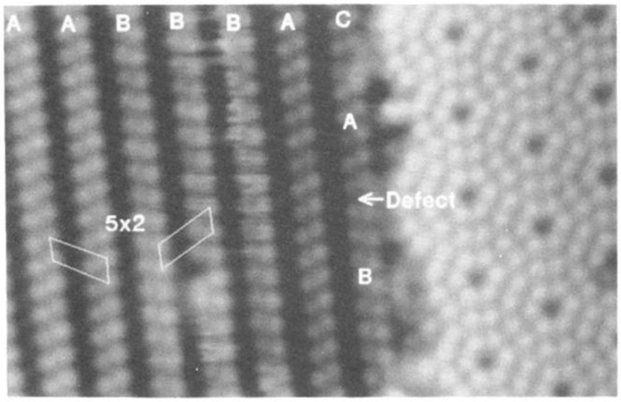

FIG. 18. Empty-state image showing both the 5×2 phase and the 7×7 structure. Rows with the two different orientations for the 5×2 unit cell (white outlines) are labeled "*A*" and "*B*."

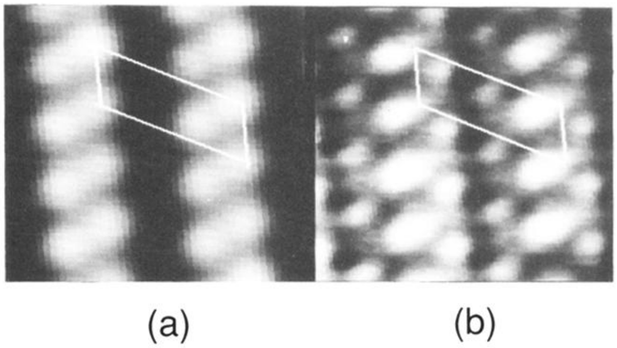

FIG. 19. Dual bias images of the 5×2 phase, taken in parallel at +1.5 V and −1.5 V sample bias, showing the (a) empty and (b) filled states of the surface. The 5×2 unit cell indicates equivalent positions of both images.

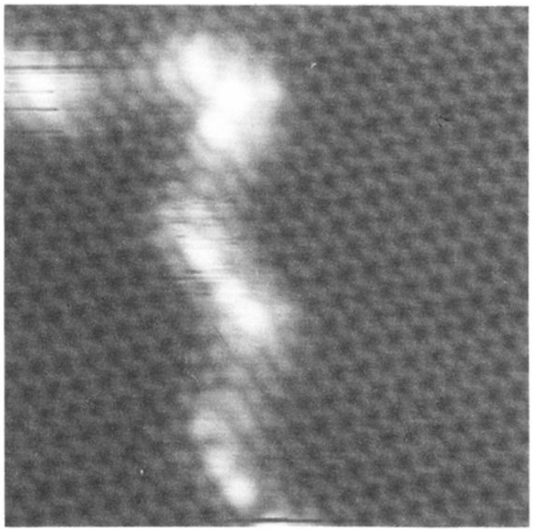

FIG. 4. Empty-states STM image showing two $\sqrt{3}\times\sqrt{3}$ domains separated by a boundary.

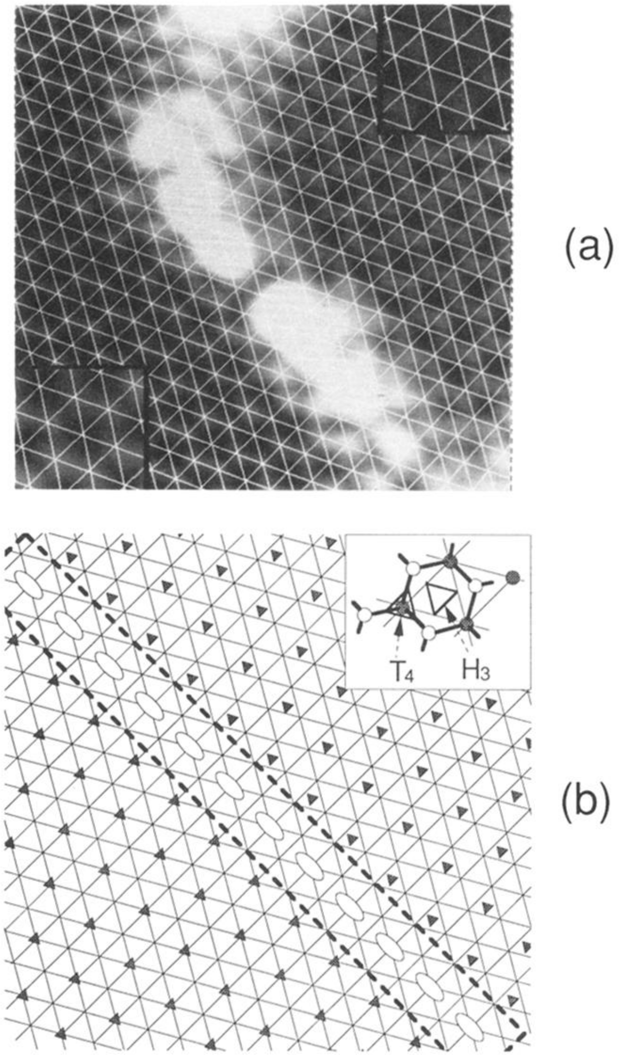

FIG. 5. (a) Portion of the image in Fig. 4 with a superimposed 1×1 grid. (b) Illustration of the shift in the registration of the $\sqrt{3}\times\sqrt{3}$ phase with respect to the grid. Dark triangles denote the positions of the Si trimers in the HCT model. The insert shows the positions of these triangles with respect to the underlying Si bilayer.

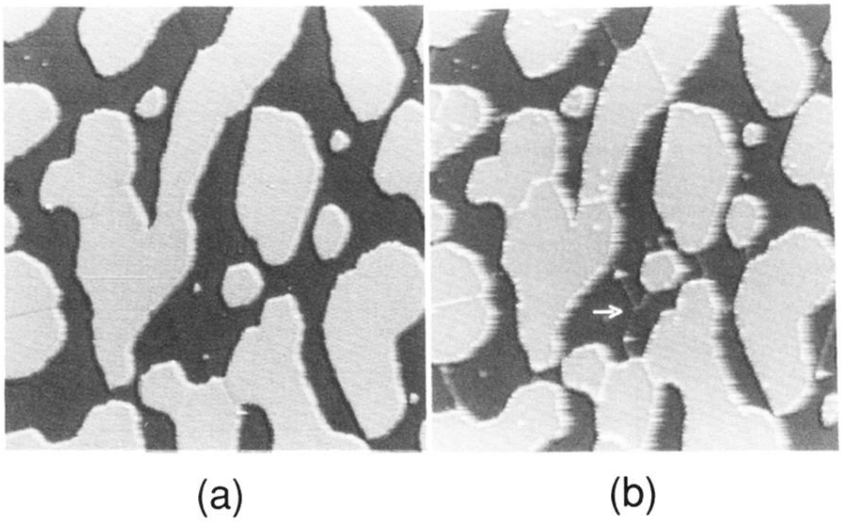

FIG. 7. Large-scale (1300×1500 Å^2) STM images of $\sqrt{3}\times\sqrt{3}$ domains, showing (a) the filled states and (b) the empty states. Both images were taken over the same sample area.

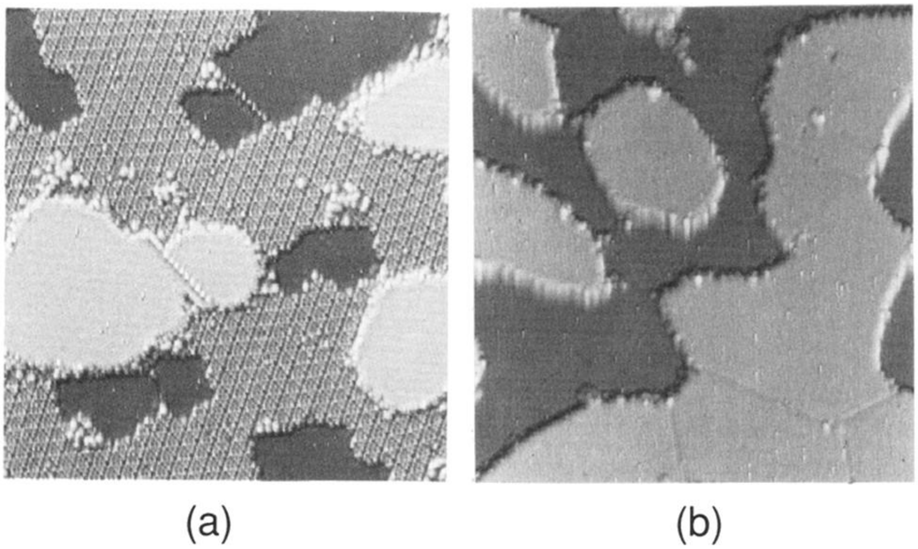
(a) (b)

FIG. 8. Ag/Si(111)-$\sqrt{3}\times\sqrt{3}$ surfaces produced at (a) 0.48 ML; (b) 1.05 ML at 400 °C.